Automatic Distributed MIMO Testbed for beyond 5G Communication Experiments

(article starts on next page)

Automatic Distributed MIMO Testbed for Beyond 5G Communication Experiments

Husileng Bao[#1], Ibrahim Can Sezgin[#2], Zhongxia Simon He[#3], Thomas Eriksson[*4], and Christian Fager[#5]

[#]Department of Microtechnology and Nanoscience, Chalmers University of Technology, Sweden

[*]Department of Electrical Engineering, Chalmers University of Technology, Sweden

{[1]husileng; [2]cani; [3]zhongxia; [4]thomase; [5]christian.fager}@chalmers.se

Abstract—**This paper demonstrates an automated testbed suitable for beyond-5G distributed MIMO experiments, where bandwidth, number of transmitters and precoding methods are flexible and configured through a central unit. This is based on an all-digital radio-over-fiber approach to communication through 12 fully coherent, low-complexity remote radio transmitters. An automated robot receiver is implemented to facilitate efficient communication data collection in realistic environments. Using the proposed system, co-located and distributed MIMO communication antenna configurations are compared in a real in-door environment. The results show that distributed MIMO provides more significantly more uniform power distribution and better overall MIMO capacity compared to co-located MIMO.**

Keywords— **remote radio head, receiver, channel capacity, distributed MIMO, co-located MIMO, statistical analysis.**

I. INTRODUCTION

Massive multiple input and multiple output (MIMO) is a key technology to increase capacity and improve energy efficiency in 5G and beyond-5G (B5G) systems [1]. By distributing the antennas in MIMO systems, the capacity and coverage can be improved.

The performance of co-located (5G) and distributed MIMO (B5G) communication has been evaluated through theoretical analysis and mathematical models in [2][3][4][5]. To experimentally evaluate the performance of new B5G wireless systems such as cell-free/distributed MIMO in complex environments, large number of measurements are needed. However, all reported testbeds have relied on manual measurements or have a small number of transmitters and receivers [6][7][8][9][10]. Naturally, these measurements become very time consuming and do not generate sufficient data for statistical purposes.

In this paper, we address this and propose a fully automated, highly flexible automated testbed for beyond-5G wireless communication experiments. By using a fully automated robot receiver, large amounts of data can be collected effectively in complex environments. Extensive statistics of channel capacity and communication performance can therefore be obtained. Previous experimental work [11] has compared performance of co-located MIMO (C-MIMO) and distributed MIMO (D-MIMO) in terms of received power and user signal quality. This is not a sufficient method to understand the true capacity potential in such systems. In this paper we therefore use the automated testbed to collect a rich amount of measurement data in an indoor environment. The data is then used to perform an extensive statistical performance comparison between C-MIMO and D-MIMO. The test results include power distribution, communication quality and channel capacity in this paper.

This paper is structured as: in section II, the testbed structure and signal processing procedures are explained. In section III, the measurement of D-MIMO and C-MIMO are discussed. The test results are presented and discussed in section IV, which is followed by a conclusion.

II. AUTOMATED DISTRIBUTED MIMO TESTBED

This section describes the details of the employed testbed. First, the testbed structure is described. Thereafter the signal processing steps are described.

A. Testbed Structure

The proposed testbed structure is illustrated in Fig. 1. The testbed utilizes all-digital radio-over-fiber for coherent distribution of radio signals [6]. A PC and an FPGA board are central unit (CU) where the signals to each remote radio head (RRH) is generated. In the CU, the computer performs offline signal processing while the FPGA transmits the generated 10 Gbps radio frequency signal over 30-meter fibers to RRUs. At RRUs, the optical signals are converted to electrical domain, amplified and radiated by RRU antennas as described in [6].
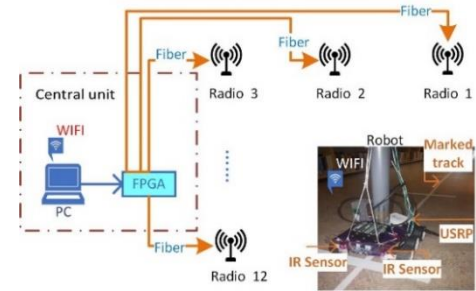

Fig. 1. An illustration of the proposed measurement testbed including the automated robot receiver. Central unit connects with 12 radios by optical fiber. Robot is equipped with an USRP which receives the signal and follows a track on the floor using IR sensors during the measurements.

The proposed testbed implements a robot receiver, which allows a large number of over-the-air (OTA) measurements. This is important to ensure that the test result has a rich statistical representation of the actual wireless communication scenario. The robot car performs three main tasks: Follow a marked track on the floor; Record the received raw data.

Transfer the raw data to the CU via WiFi connection after each measurement.

The robot comprises a Raspberry Pi 3 Model B [12] and An USRP B205mini-i radio front end [13] is the receiver, which is controlled by Raspberry Pi. The USRP captures IQ data at 56 Msym/s. The Raspberry Pi has WiFi connectivity which exchanges control commands and measurement data with the CU. The robot car is supplied by battery pack and power bank which can support operation up to 8 hours.

B. Signal Processing Procedure

At each measurement location, signal processing for MIMO channel estimation (7 steps) and MIMO communication (9 steps) are performed, as Fig. 2. For Step 1 of the channel estimation, only one RRU transmits signal at a given time. Robot car down converts and filters the pilot signal at Step 2. Since the oscillators at transmitter and receiver are unsynchronized, frequency offset adjustment is performed, followed by resampling, preamble detection and matched filtering through Steps 3-5. The baseband signals are obtained after the timing adjustment and down-sampling in Step 6.

The received complex baseband signal, denoted by y, can be expressed as below

$$y = XH + w. \qquad (1)$$

where X is the training pilot data, H is the channel matrix and w is an additive noise. With known pilots X and captured signal y, the H can be estimated by a least square method

$$\hat{H} = (X^T X)^{-1} X^T y. \qquad (2)$$

After channel estimation, MIMO communication test is also performed. With estimated channel information $\hat{H}$ the user data u is generated in Step 8. Zero-forcing precoding transforms the user data into transmitter data M to the antennas in Step 9 by multiplying the user data u with Moore–Penrose inverse of channel matrix $\hat{H}$:

$$M = (\hat{H}\hat{H}^*)^{-1} \hat{H} u. \qquad (3)$$

The MIMO data m is transmitted at Step 10 and robot car receives it at Step 11. Step 12-15 are corresponding to frequency offset adjustment, resample and preamble detection, matched filtering and timing adjustment and down sample. In Step 16, the amplitude and phase of the received baseband MIMO signal is adjusted, saved and transferred back to CU as the raw data of the measurement.
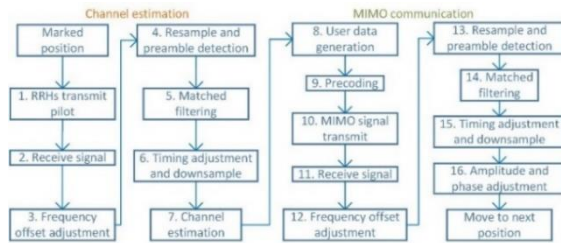

Fig. 2. Flowchart for the testbed operation. At marked position the robot stops, and channel estimation and MIMO communication tests are performed.

III. INDOOR MEASUREMENT

To exemplify the capabilities of the testbed, C-MIMO and D-MIMO measurement has been done in an indoor office

environment illustrated in Fig. 3. For the C-MIMO case, all the 12 RRHs are set up together. For the D-MIMO case, RRHs are equally deployed around the measurement area as indicated in Fig. 3. The robot car follows a track from position 1-44, with positions 26-33 inside a conference room (see Fig. 3). At each position, channel estimation and MIMO communication measurements are performed for a 5 Mbaud, 64 QAM signal at 2.365 GHz. The only difference between two cases is the distribution of RRHs.

Fig. 3. Indoor layout for measurement. Green and orange antennas represent placement of distributed- and co-located antennas, respectively. Whole area is enclosed by walls and there are boards, tables, chairs and a conference room. The numbered blue circles are measurement positions.

IV. MEASUREMENT RESULTS

Received power distribution and normalized mean square error (NMSE) are used as figures of merit for single user communication in section A. Furthermore, the estimated channel matrix allows us to analytically compare multi-user MIMO capacity limits for the C-MIMO and D-MIMO.

A. Power Distribution and received signal quality

Fig. 4 presents the received power distribution and NMSE. As shown in Fig. 4 the received power varies from -30 to -80 dBm for C-MIMO while D-MIMO has a lower power variation of -40 to -60 dBm. In the C-MIMO case, the power drops significantly for position 25-33, inside the conference room area of Fig. 3. Clearly, the power distribution is more equally in the distributed measurement which helps to reduce receiver dynamic range requirements compared to C-MIMO.

Fig. 4 also shows that NMSE fluctuates between -20 ~ -30 dB for both C-MIMO and D-MIMO. The mean value of NMSE for C-MIMO and D-MIMO is -24.0 dB and -23.7 dB, respectively. This means that there is no apparent difference between them with stable communication in both cases.
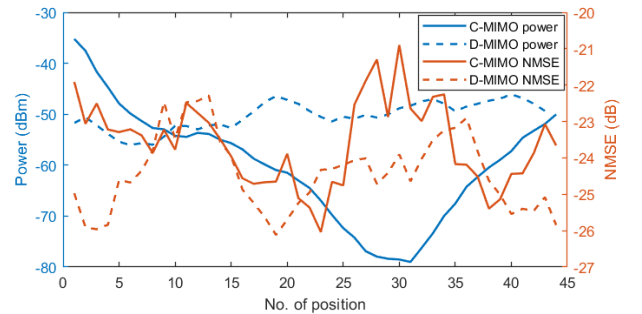

Fig. 4. Power distribution and NMSE for each position. Solid line represents C-MIMO and dashed line shows D-MIMO. Blues curves are power and orange curves are NMSE.

B. *Channel Capacity*

With knowledge about the channel matrix, it is possible to estimate the capacity limits for multiple users. The expression for the user capacity in such a case is given by [14],

$$C_m \;=\; log_2\left(1 + \sigma_m^2 \frac{S}{BN_0}\right). \tag{4}$$

where C_m is capacity for user m [bit/s/Hz], S is transmitted signal power, B is signal bandwidth, and N_0 represent noise power density. σ_m^2 is the channel weight and is the mth eigenvalue obtained by singular value decomposition of the 12×M MIMO channel matrix.

A generic scenario with 50000 randomized sets of 4 user locations among the 44 positions have been considered. The corresponding user capacities have been determined from (4) using eigenvalues obtained from decomposition of the measured channel matrices. The calculations have assumed an output power and noise ratio, $S/(BN_0) = 30$ dB, at the best overall user position. Fig. 5 compares the user capacities of the C-MIMO and D-MIMO.

The results in Fig. 5 shows clear differences between C-MIMO and D-MIMO. Firstly, there are more users in the low capacity range, with <5 bit/s/Hz, in C-MIMO than in D-MIMO although a few users may have higher capacity in the C-MIMO case. Secondly, in the capacity range 4-10 bit/s/Hz, D-MIMO has more users than C-MIMO. Clearly, D-MIMO, in general, serves users with a more uniform high capacity.
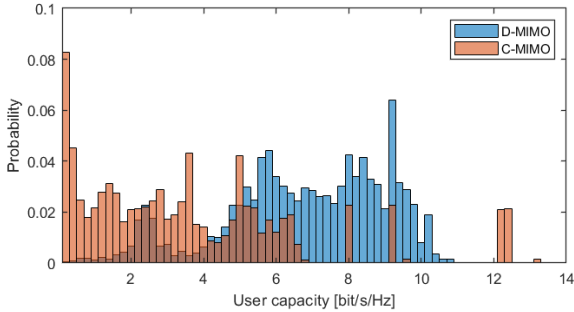

Fig. 5. Histogram of estimated user capacity in a 4-user MIMO indoor scenario for a co-located (C-MIMO) and distributed (D-MIMO) antenna setting. The number of users for each section is normalized to get probability.

The capacity in one location depends on the location of the other three users. Fig. 6 illustrates the user capacity distribution as a box-plot organized versus location. The capacity in C-MIMO shows a large variation depending on the position of the other users, particularly for positions 1-4 which are close to the base station. The capacity for locations far away from C-MIMO antennas have low capacity, particularly in the conference room area (see Fig. 3). D-MIMO can, on the other hand, promise a stable capacity for all of the positions. The median capacity of each position also shows that D-MIMO has medium capacity greater than 5 bit/s/Hz while C-MIMO has an overall significantly lower capacity. These results represent one of the first experimental verifications of the theoretical studies in [2][3][4][5].
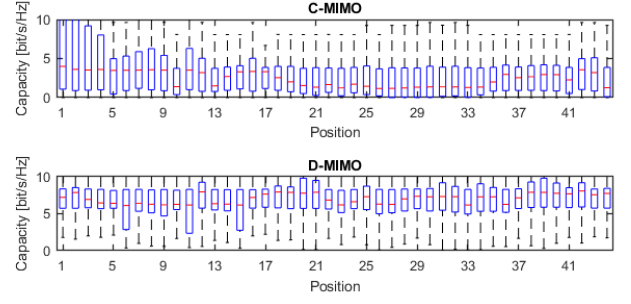

Fig. 6. User capacity distribution at each position for C-MIMO and D-MIMO. The blue rectangles represent the 25th to 75th percentile of the capacity. The red line represents the median capacity.

V. CONCLUSION

This paper has presented an automated radio testbed suitable for D-MIMO indoor applications. The indoor measurement conclusion, indoor is that D-MIMO can cover users with more uniform power than C-MIMO. Furthermore, the measured channel characteristics have been used to determine that D-MIMO has almost twice the median capacity and in particular more uniform capacity compared with C-MIMO in a realistic indoor environment.

REFERENCES

[1] H. Q. N. Thomas L. Marzetta, *Fundamentals of massive MIMO*. Cambridge University Press, 2016.

[2] Z. Liu and L. Dai, "Asymptotic capacity analysis of downlink MIMO systems with co-located and distributed antennas," *IEEE Int. Symp. Pers. Indoor Mob. Radio Commun. PIMRC*, pp. 1286–1290, 2013, doi: 10.1109/PIMRC.2013.6666337.

[3] M. K. Bhatt and M. P. Shah, "located and distributed antenna configuration," no. Icici, pp. 458–461, 2017.

[4] A. S. Konanur, K. Gosalia, S. H. Krishnamurthy, B. Hughes, and G. Lazzi, "Increasing wireless channel capacity through MIMO systems employing co-located antennas," *IEEE Trans. Microw. Theory Tech.*, vol. 53, no. 6 I, pp. 1837–1843, 2005, doi: 10.1109/TMTT.2005.848105.

[5] L. Xiao, L. Dai, H. Zhuang, S. Zhou, Y. Yao, and A. D. A. S. T. Model, "Inforrnat ion- t heore t ic Capacity Analysis in MIMO Distributed Antenna Systems," no. 1, pp. 779–782.

[6] I. C. Sezgin *et al.*, "A Low-Complexity Distributed-MIMO Testbed Based on High-Speed Sigma-Delta-Over-Fiber," *IEEE Trans. Microw. Theory Tech.*, vol. 67, no. 7, pp. 2861–2872, 2019, doi: 10.1109/TMTT.2019.2904265.

[7] I. Jones and G. G. Raleigh, "Channel estimation for wireless OFDM system," vol. 81, 1998.

[8] C. Y. Wu *et al.*, "Distributed Antenna System Using Sigma-Delta Intermediate-Frequency-Over-Fiber for Frequency Bands above 24 GHz," *J. Light. Technol.*, vol. 38, no. 10, pp. 2764–2772, 2020, doi: 10.1109/JLT.2020.2976605.

[9] K. M. Asudaria, "Reconfigurable Testbed Communication System," no. Icoei, pp. 372–377, 2020.

[10] Huaiyu Dai, "DISTRIBUTED VERSUS CO-LOCATED MIMO SYSTEMS WITH CORRELATED FADING AND SHADOWING Department of Electrical and Computer Engineering , NC State

University , Raleigh , NC 27695 Email : Huaiyu_Dai@ncsu.edu," pp. 561–564, 2006.

[11] I. C. Sezgin, T. Eriksson, J. Gustavsson, and C. Fager, "Evaluation of Distributed MIMO Communication Using a Low-Complexity Sigma-Delta-over-Fiber Testbed," *IEEE MTT-S Int. Microw. Symp. Dig.*, vol. 2019-June, pp. 754–757, 2019, doi: 10.1109/mwsym.2019.8700985.

[12] (2020) Raspberry Pi 3 Model B webpage on Raspberry Pi. [Online]. Available: https://www.raspberrypi.org/products/raspberry-pi-3-model-b/.

[13] "USRP B200mini Series Datasheet," Ettus Research, Santa Clara, California, USA.

[14] Vucetic, Branka, and Jinhong Yuan. Space-time coding. John Wiley & Sons, 2003.